Applied Catalysis B: Environmental 148–149 (2014) 499–508

Contents lists available at ScienceDirect

Applied Catalysis B: Environmental

journal homepage: www.elsevier.com/locate/apcatb

New bifunctional catalytic systems for sorbitol transformation into biofuels

Léa Vilcocq[a], Régis Koerin[a], Amandine Cabiac[a,*], Catherine Especel[b], Sylvie Lacombe[a], Daniel Duprez[b]

[a] IFP Energies nouvelles, rond-point de l'échangeur de Solaize, BP 3, 69360 Solaize, France
[b] IC2MP (Institut de Chimie des Milieux et Matériaux de Poitiers), Université de Poitiers, UMR 7285 CNRS, 4 rue Michel Brunet, 86022 Poitiers Cedex, France

ARTICLE INFO

Article history:
Received 19 April 2013
Received in revised form
12 November 2013
Accepted 13 November 2013
Available online 21 November 2013

Keywords:
Sorbitol
Aqueous medium
Tungstated oxides
ZrO_2–WO_x
Al_2O_3–WO_x
TiO_2–WO_x
Dehydration
Hydrogenation

ABSTRACT

Tungstated oxides were prepared from several supports and characterized. The tungsten surface repartition and availability depends on the initial support. The acidity in water was evaluated through a model compound reaction, cyclohexanol dehydration. The results show that acidity in water is completely different from gas phase acidity (from NH_3-TPD), evidencing the crucial role of water in the acid catalytic activity. The tungstated oxides were then mixed with Pt/ZrO_2 to obtain a bifunctional catalytic system, which was used for transforming sorbitol in water. The activity and selectivity is highly dependent on the acid phase. TiO_2–WO_x led to increased activity and higher selectivity for long chain hydrocarbons (C5-C6 alkanes) which can be valorized as biofuels, when compared to traditional sorbitol transformation catalyst. Al_2O_3–WO_x is not acid in water but produces short alcohols by C—C cleavage. These results provide an incentive for further catalysts preparation.

1. Introduction

In the present context of oil demand increase and growing interest for sustainable development, biomass, an abundant and renewable material, appears as an attractive resource for energy and particularly for fuel production [1]. A promising way to produce hydrocarbons from biomass is the direct transformation of lignocellulosic sugars or polyols into hydrocarbons, using a bifunctional heterogeneous catalyst [2–4]. Sorbitol is one of the most studied polyol. It is also part of the twelve ex-biomass compounds identified as valuable starting materials for fuels or chemicals production by the American department of energy (DOE) [5,6]. It can be produced by catalytic hydrogenation of glucose [7,8] or directly from cellulose [9–11]. Several metal/acid catalytic systems have been described in the literature for sorbitol transformation [12]: Pt/SiO_2–Al_2O_3 [3,13,14], Pd/SiO_2–Al_2O_3 [3], Pt/Nb_2O_5 [15], Pt/Nb_2O_5–PO_x [15], Pt/ZrO_2–PO_x [16], and Ni/H–ZSM5 [17].

Our previous works [18,19] concerned a Pt/SiO_2–Al_2O_3 catalyst for sorbitol transformation. We described the behavior of the metallic and acid phases in water, determined the optimal Pt content for hydrocarbons production and proposed a general scheme for the reaction (Fig. 1). Our conclusions were that this catalyst is not suitable for sorbitol dehydration–hydrogenation in water because its physical and chemical properties are strongly affected by the hydrothermal medium and its decarbonylating activity leads to a significant CO_2 yield, not suitable for the high atom economy required in green processes.

In this paper, new heterogeneous catalytic systems are designed by changing the nature of the acid phase. The aim is to identify an acid solid that would be both stable in hydrothermal conditions and selective for sorbitol transformation into C5-C6 alkanes when associated with a Pt-based metallic catalyst. For this purpose, mechanical mixtures were prepared in order to separate the Pt metallic phase supported on the same stable oxide (ZrO_2) and the various acid phases, which guarantees that the metallic phase presents the same characteristics in terms of particle size, acid site-metallic site distance, etc., whatever the combined acid phase.

The hydrothermal stability was a decisive criterion for the choice of the acid solids. For this reason, zeolites [20,21] and silica–aluminas [18] were not selected. Mixed oxides, e.g., ZrO_2–TiO_2 and ZrO_2–Al_2O_3, and transition metals over oxides, present better stability during aqueous phase reactions [16,22,23]. Among them, tungstated oxides have shown interesting activity and stability in aqueous phase biomass valorization processes [24].

* Corresponding author. Tel.: +33 4 37 70 22 26.
E-mail address: amandine.cabiac@ifpen.fr (A. Cabiac).

0926-3373/$ – see front matter © 2013 Elsevier B.V. All rights reserved.
http://dx.doi.org/10.1016/j.apcatb.2013.11.016

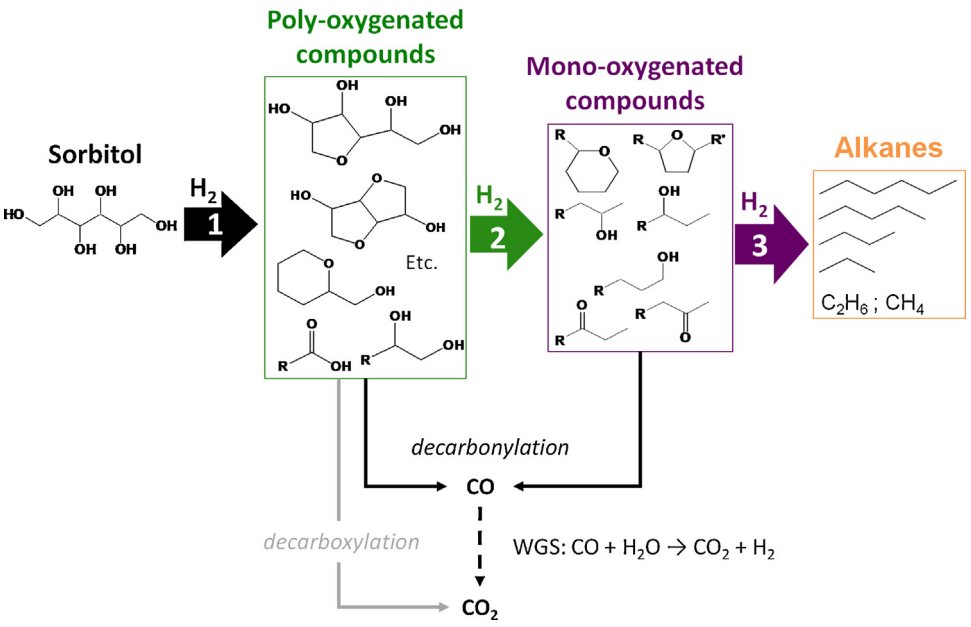

Fig. 1. Sorbitol transformation: general scheme (WGS: water gas shift reaction).

Three tungstated oxides were therefore selected as acid catalysts: ZrO_2–WO_x, TiO_2–WO_x, and Al_2O_3–WO_x.

The characterization of the monofunctional acid catalysts and their behavior in hydrothermal conditions are presented. Acidity in gas phase was evaluated through temperature programmed ammonia desorption (NH_3-TPD) whereas acidity in aqueous phase was evaluated through a cyclohexanol dehydration test. Concerning sorbitol transformation, a metallic Pt/ZrO_2 catalyst mixed with silica–alumina (reference acid phase) was tested in a first step to validate the mechanical mixing protocol. In a second step, Pt/ZrO_2 was mixed with each of the three studied tungstated oxides to identify an optimal acid phase.

2. Experimental part

2.1. Catalyst preparation

2.1.1. Tungstated oxides

Tungstated oxides were prepared by ionic exchange on $Zr(OH)_4$ (MEL Chemicals), boehmite AlOOH (Pural SB3 Condea), and TiO_2 rutile supports. TiO_2 oxide was prepared by $TiCl_4$ thermolysis in HCl solution from [25]. $ZrOH_4$ and AlOOH were chosen instead of ZrO_2 and Al_2O_3 to facilitate both the tungsten deposit and the final extrusion. 50 mL of a H_2WO_4 in H_2O_2 30% v/v solution (0.25 mol L^{-1}) were added to 10 g of dry support dispersed in 75 mL of water and stirred overnight. The solution was centrifuged (30 min, 8000 rpm). The recovered solid was dried (80 °C, 18 h). The $Zr(OH)_4$–WO_x and AlOOH–WO_x were then extruded. The solids were calcined during 3 h at 700 °C (ZrO_2–WO_x), 650 °C (Al_2O_3–WO_x) or 600 °C (TiO_2–WO_x). The calcination temperatures were optimized during a preliminary work in order to obtain the proper crystallographic structure with maximal surface area (γ-Al_2O_3, mainly tetragonal ZrO_2 and rutile TiO_2).The extrudates were finally crushed and sieved (grain size 150–355 μm, chosen on the basis of preliminary diffusion limitation studies).

2.1.2. Platinum catalyst

Platinum was deposited on silica–alumina extrudates (siralox30, SASOL, 30 wt.% silica) or on zirconia extrudates (MEL Chemicals) by incipient wetness impregnation using aqueous solution of H_2PtCl_6 (Alfa Aesar). The impregnated catalysts were dried at 120 °C during 5 h, and then calcined at 520 °C, 2 h under air flow. The metallic catalyst 2.2 wt.% Pt/ZrO_2 has a BET specific surface area of 79 m^2 g^{-1}, its porous volume is 0.22 mL g^{-1} and its mesopores diameter is centered on 8.3 nm. They were finally milled and sieved to be used as grains (size 150–355 μm) in the sorbitol transformation test.

2.1.3. Mechanical mixtures

The 2.4 wt.% Pt/SiO_2–Al_2O_3 + SiO_2–Al_2O_3 reference catalyst was prepared by milling the extrudates of both catalysts together in a 50:50 mass ratio. The 150–355 μm fraction was collected by sieving. The other bifunctional catalytic systems were prepared by mixing the (150–355 μm) grains of an acid catalyst (ZrO_2–WO_x, Al_2O_3–WO_x or TiO_2–WO_x) and the Pt/ZrO_2 metallic catalyst in a 10 mL flask. The proportions were 4 g of acid phase and 2 g of metallic phase.

2.2. Catalyst characterization

All the tungstated oxides characterizations were performed after the calcination step described in Section 2.1. Raman spectra were obtained on a Lab Ram ARAMIS (HORIBA Jobin-Yvon) spectrometer equipped with a CCD detector and an Nd-YAG laser with a wavelength of 532 nm and a 5 mW power. The focus was ×50 LWD, giving a focal point of 2 μm. Scanning electron microscopy (SEM) pictures were obtained with Zeiss Supra 40 apparatus. SEM was used in topological contrast and in chemical contrast. X-ray diffraction (XRD) was performed on a Panalytical (XPert Pro) device. The amount of acid sites was determined by ammonia temperature-programmed desorption (NH_3-TPD) in an Autochem II 920 (Micromeritics): the catalyst sample was first pre-treated under helium flow at 400 °C for 1 h, then cooled to 150 °C and ammonia-saturated in a stream of 10% NH_3/He flow (50 mL min^{-1}) for 0.5 h. After purge under helium at 150 °C for 0.5 h, ammonia was desorbed using a linear heating rate of 10 °C min^{-1} to 600 °C. Desorbed ammonia was analysed on a TCD detector. The BET specific surface area and the pore volume of the catalysts were determined by nitrogen isothermal adsorption–desorption at −196 °C using an ASAP 2420 (Micromeritics), after calcination at 350 °C, 3 h. Platinum, zirconium, aluminium, titanium, and tungsten contents

were determined by X-ray fluorescence with a PW2404 Phillips (Panalytical) device.

2.3. Catalytic tests

2.3.1. Cyclohexanol dehydration

The cyclohexanol dehydration reaction was used to evaluate the acidity of the catalysts in aqueous medium. The catalyst (150–355 μm, 2.5 g) was placed in a 500 mL autoclave with 250 mL of an aqueous solution of cyclohexanol 10 g kg^{-1}. The autoclave was heated at 240 °C during 2 h and stirred at 800 rpm. The absence of external diffusion limitations was verified by testing several stirring rates. Samples were taken regularly and cyclohexanol was analyzed by GC–FID.

2.3.2. Sorbitol transformation

The sorbitol transformation reaction was carried out in a fixed-bed reactor already described [19]. Prior to reaction, the fresh catalyst was reduced under hydrogen flow (3 L h^{-1} $g_{cat}{}^{-1}$) at 450 °C for 2 h. The 10 wt.% aqueous solution of sorbitol was introduced with hydrogen co-feeding. The weight hourly space velocity (WHSV) was based on the aqueous solution of sorbitol: WHSV = (mass flow rate of feed solution)/(mass of catalyst). Four sets of operating conditions were successively applied during each test: 200 °C, 22 bar, WHSV = 2 h^{-1}; 220 °C, 29 bar, WHSV = 2 h^{-1}; 240 °C, 37 bar, WHSV = 2 h^{-1}; 240 °C, 37 bar, WHSV = 4 h^{-1}. The average time-on-stream was one week. Each set of operating conditions has been studied for hours (max 15 h) with several sampling of gas and liquid phases and no decrease in activity was observed for any of the catalytic systems.

At the end of the test, the spent catalyst was rinsed with degassed water during 3 h at 240 °C, 36 bar under nitrogen flow, and stripped with nitrogen under the same conditions. It was then dried overnight at 110 °C, then unloaded and separated from SiC by sieving. The eventual deposited carbon on the spent catalyst was checked in all cases by elemental analysis. Before characterisation (nitrogen adsorption–desorption), the spent catalyst was progressively calcined at 500 °C under diluted air with an exothermicity control at less than 2 °C, in order to prevent any support and/or metallic phase sintering during eventual carbon burning. The objective was to see any modification of the texture support, and not to evaluate the accessible porosity during the test. The analytical methods on the effluent and way of calculating the carbon balance, the sorbitol conversion and the yields in the various products were described previously [19].

3. Results and discussion

3.1. Tungstated oxides characterizations

Table 1 gives the results of physical and chemical characterizations of the three prepared tungstated oxides and the reference silica–alumina. The tungsten content varies from 8.6 wt.% (for Al_2O_3–WO_x) to 14.7 wt.% (for TiO_2–WO_x), showing that the ionic exchange ratio is highly dependent on the support and mainly on the hydroxylation rate.

3.1.1. Raman spectroscopy

Raman spectroscopy helps to identify the tungsten species on the catalyst surface by the vibrations of the chemical bonds between the W atom and its environment.

Fig. 2a represents the Raman spectra obtained on the tungstated zirconia at different spots on the sample. The bands below 700 cm^{-1} are attributed to the ZrO_2 support. Two important signals at 960 and 990 cm^{-1} are observed, attributed to a ν(W=O)

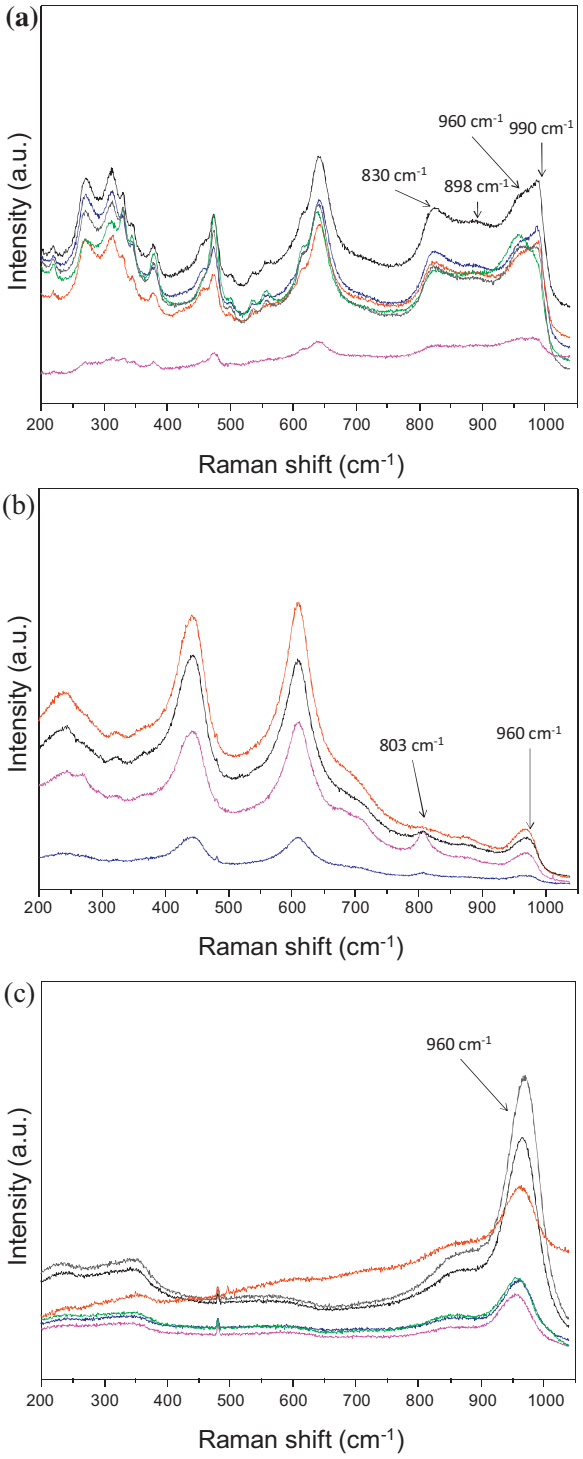

Fig. 2. Raman spectra of (a) ZrO_2–WO_x tungstated zirconia, (b) TiO_2–WO_x tungstated titania, (c) Al_2O_3–WO_x tungstated alumina. Each color represents an individual spectra collected at one spot of the sample.

stretching vibration mode of poly-tungstated species in a pentahedral environment [26]. The first band corresponds to highly dispersed species; the second one is attributed to less dispersed species, the 30 cm^{-1} shift showing a condensation phenomenon. Two other bands at 830 and 898 cm^{-1} are attributed to ν(W—O—W) and ν(W—O—Zr) vibration modes, respectively.

Fig. 2b shows the spectra obtained on tungstated titania. The bands below 700 cm^{-1} are attributed to the titania support. All the spectra present a 960 cm^{-1} band which can be attributed to a

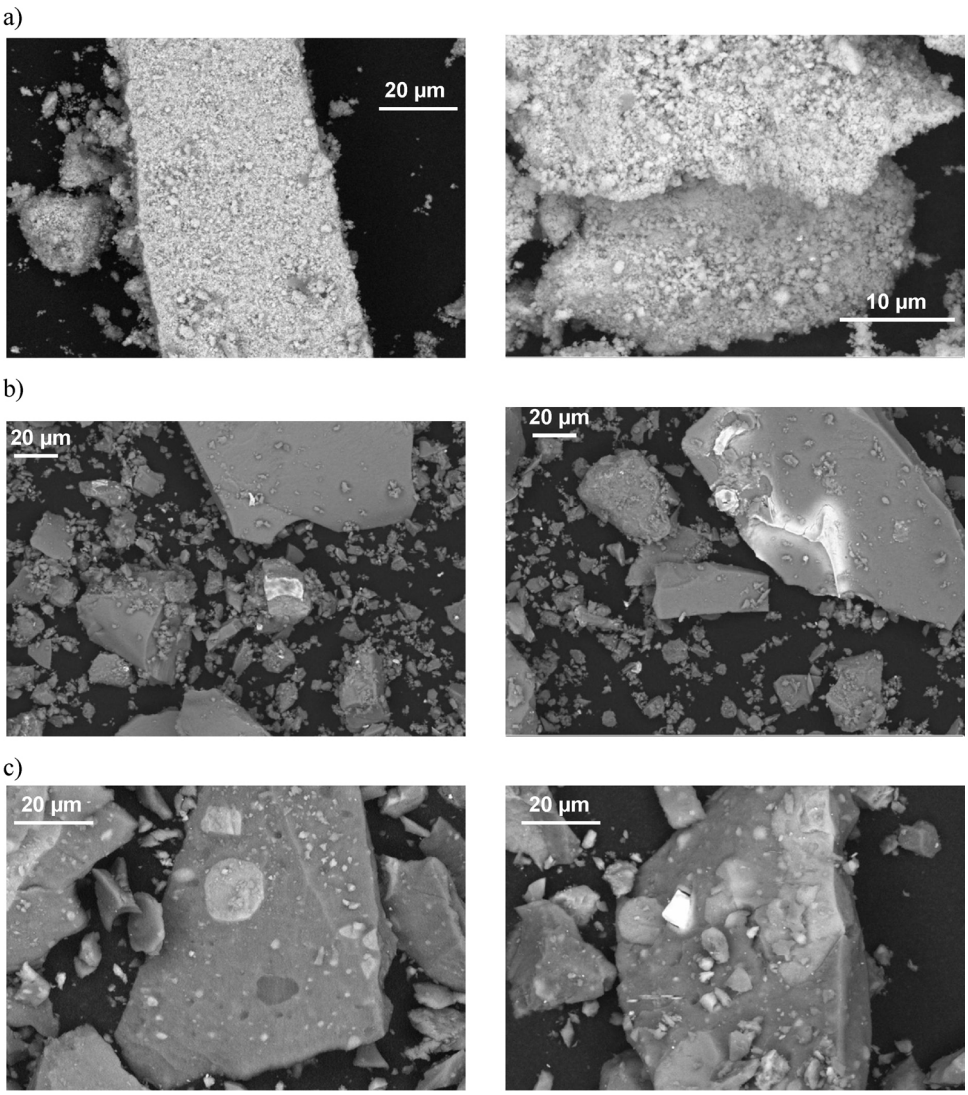

Fig. 3. SEM pictures in chemical contrast of (a) ZrO_2–WO_x, (b) TiO_2–WO_x and, (c) Al_2O_3–WO_x. The chemical contrast technique colors the tungsten in light grey-white and the supports in dark grey.

ν(W=O) stretching vibration mode of poly-tungstated species in a pentahedral environment. On one of the spectra, a band at 803 cm^{-1} can be seen, attributed to tungsten in an octahedral environment, in WO_3 crystallites [26].

In the case of tungstated alumina (Fig. 2c), the spectra contain mainly an important signal at 960 cm^{-1}, attributed to a ν(W=O) stretching vibration mode of poly-tungstated species in a pentahedral environment, highly dispersed.

Pentahedral tungsten species are thus observed over all three tungstated oxides highly dispersed in most cases. For ZrO_2–WO_x, moderately dispersed pentahedral species coexist with highly dispersed ones. For TiO_2–WO_x, WO_3 octahedral species are present too, although in minority and heterogeneously localized on the catalyst surface.

Although the tungsten loading is high, the Raman spectroscopy does not evidence any WO_3 crystalline species, except in minority on TiO_2 surface. XRD diffractograms (not shown) do not show any trace of WO_3 crystallite neither. The W coverage for ZrO_2–WO_x, TiO_2–WO_x, and Al_2O_3–WO_x is respectively 5.5, 4.6, and 1.3 W atoms nm^{-2}, which is below the value of 6–10 W atoms nm^{-2} commonly accepted for the formation of WO_3 crystallites [27,28].

Table 1
Physical and chemical properties of the tungstated oxides and of the reference silica–alumina.

Catalyst	ZrO_2–WO_x	TiO_2–WO_x	Al_2O_3–WO_x	SiO_2–Al_2O_3
W content (wt.%)	13.9 ± 0.3	14.7 ± 0.3	8.6 ± 0.2	–
Crystalline phase	ZrO_2 tetragonal (+ ZrO_2 monoclinic)	TiO_2 rutileWO_3	γ-Al_2O_3	γ-Al_2O_3
BET surface area ($m^2\,g^{-1}$)	84	106	237	318
Pore volume ($mL\,g^{-1}$)	0.21	0.37	0.50	0.66
Mean pore diameter (nm)	4.9	12.0	6.5	7.1
Total acidity ($\mu mol_{NH3}\,g^{-1}$)[a]	201	320	349	290

[a] Acidity measured by NH_3-TPD after calcination.

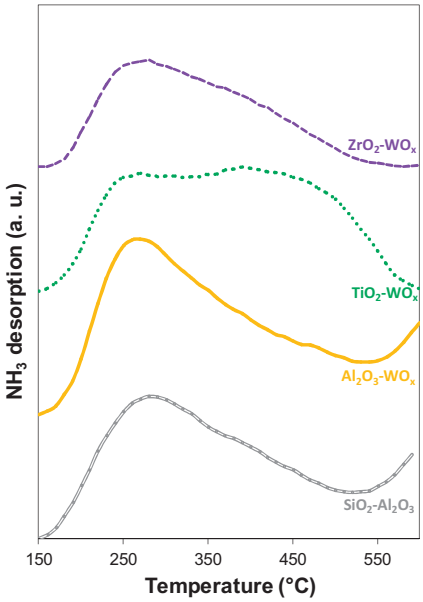

Fig. 4. Ammonia-temperature programmed desorption (NH_3-TPD) profiles of SiO_2–Al_2O_3, ZrO_2–WO_x, TiO_2–WO_x, and Al_2O_3–WO_x.

3.1.2. Scanning electron microscopy

The tungstated oxides were characterized by SEM using chemical contrast, after reduction at 450 °C. The picture of ZrO_2–WO_x (Fig. 3a) shows a homogeneous tungsten distribution. In the case of TiO_2–WO_x (Fig. 3b), a heterogeneous tungsten distribution clearly appears. For Al_2O_3–WO_x (Fig. 3c), a tungsten-rich phase is present in the form of compact spherical inclusions. The size of these inclusions can reach 80 μm. Some "faceted" particles are also present. This is in contrast with Raman spectroscopy results which did not give any evidence of these inclusions. This contradiction is attributed to the difference in analysis depth between both techniques: the tungsten clusters are not analyzed by Raman spectroscopy because they are under the surface of the catalyst. The SEM in chemical contrast shows these inclusions because it reaches a deeper layer under the catalyst surface.

3.1.3. Acidity in gas phase: NH_3-TPD

The characterization of acid catalysts with NH_3-TPD gives an estimation of the acid sites number and strength in gas phase. However, NH_3-TPD does not allow differentiating Brønsted and Lewis acid sites. All desorption profiles, this of SiO_2–Al_2O_3 included, contain a large peak of ammonia desorption before 350 °C attributed to weak acid sites (Fig. 4). The concentration of these weak acid sites per gram of catalyst in the range [150–350 °C] gives the following decreasing ranking:

$$Al_2O_3 - WO_x > SiO_2 - Al_2O_3 > TiO_2 - WO_x > ZrO_2 - WO_x.$$

Ammonia desorption after 350 °C is attributed to stronger acid sites. The concentration of these strong acid sites per gram of catalyst in the range [350–550 °C] gives the following decreasing ranking:

$$TiO_2 - WO_x > Al_2O_3 - WO_x \approx SiO_2 - Al_2O_3 > ZrO_2 - WO_x.$$

It is important to note that a part of the measured acid sites may come from the oxide support rather than from the supported tungsten. Indeed, titania and zirconia are known as weakly acid catalysts [29,30] holding weak acid sites (ZrO_2 [31]) or weak to medium acid sites (TiO_2 rutile [31]). The acidity measured by NH_3 TPD of a γ-alumina with a BET specific surface area of 150 $m^2\,g^{-1}$ is

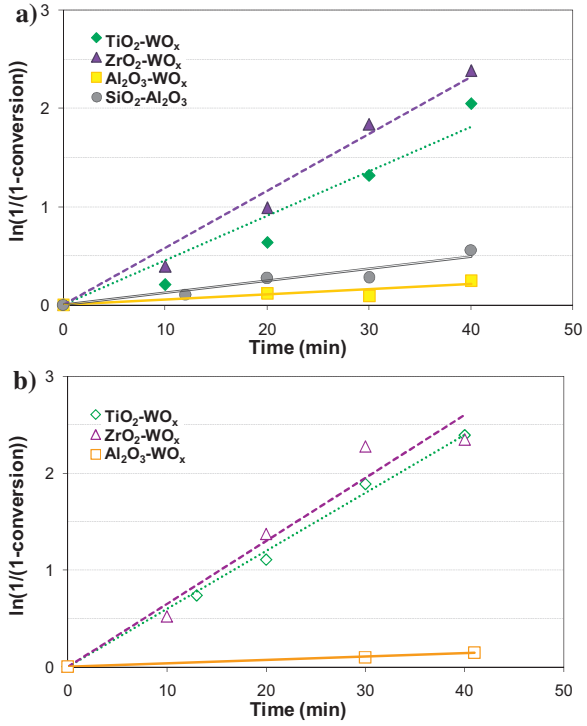

Fig. 5. Cyclohexanol dehydration test: ln(1(1-conversion)) as a function of time for (a) the calcined acid catalysts and (b) the reduced acid catalysts.

200 $\mu mol_{NH_3}\,g^{-1}$, i.e., 1.3 $\mu mol_{NH_3}\,m^{-2}$, with mainly weak acid sites. The Al_2O_3–WO_x oxide studied here contains 1.5 $\mu mol_{NH_3}\,m^{-2}$.

The area under the curves of Fig. 4 can be divided more precisely into four zones, giving a ranking of acidity with very weak acid sites (150–250 °C), weak acid sites (250–350 °C), strong acid sites (350–450 °C), very strong acid sites (450–550 °C) (Fig. S2).

Different acidity profiles appear: (i) silica–alumina, tungstated alumina, and tungstated zirconia contain a majority of weak acid sites and a minority of very strong acid sites, (ii) tungstated zirconia has fewer weak acid sites than the other catalysts in all categories, and (iii) tungstated titania contains the biggest amount of strong and very strong acid sites.

3.1.4. Acidity in liquid phase: cyclohexanol dehydration

The acidity of the tungstated oxides under hydrothermal conditions was evaluated using as model reaction cyclohexanol dehydration towards cyclohexene in aqueous phase in a batch reactor. Cyclohexanol was chosen among alcohols with six carbon atoms, preferentially to hexanol that is less soluble in water (6 $g\,L^{-1}$ versus 40 $g\,L^{-1}$ at room temperature).

In a first step, the acid catalysts were tested as prepared (Fig. 5a). The tungstated zirconia and titania are clearly more active than the reference silica–alumina; the tungstated alumina has the lowest activity, which can be explained by the presence of tungsten inclusions previously observed by SEM. The acid activity varies with the support, following the decreasing ranking in activity:

$$ZrO_2 - WO_x > TiO_2 - WO_x >> SiO_2 - Al_2O_3 >> Al_2O_3 - WO_x.$$

It is obvious that this ranking is completely different from the one established in gas phase with NH_3-TPD measurements. Indeed, tungstated alumina and silica–alumina both exhibit an important amount of acid sites in gas phase whereas their activity in aqueous phase is very low. A strong adsorption of water on the acid sites of tungstated oxide could be responsible for this phenomenon, as previously described [32]. The high dispersion of tungsten on zirconia, associated with strong tungsten-support interaction, can also lead

to an increase in the concentration in strong acid sites [33], which seem active in water.

In a second step, the tungstated oxides were tested after reduction at 450 °C during 2 h, under hydrogen flow (Fig. 5b). An acidity leveling occurs for TiO_2–WO_x and ZrO_2–WO_x which exhibit now a similar high activity, higher than after calcination. Al_2O_3–WO_x is still poorly active.

3.2. Acid phase stability in the aqueous reaction medium

As previously mentioned, the tungstated oxides have been mechanically mixed with the metallic 2.2 wt.% Pt/ZrO_2 catalyst (cf. Section 2.1) for sorbitol transformation. The support is a commercial zirconia (MEL Chemicals) with a monoclinic structure. After test, the dissociation of the two components of the mechanical mixing being impossible, the characterizations were performed on the overall mechanical mixings (Table 2). The theoretical values of the fresh mechanical mixings calculated from the characterizations of the monofunctional catalysts are given into brackets.

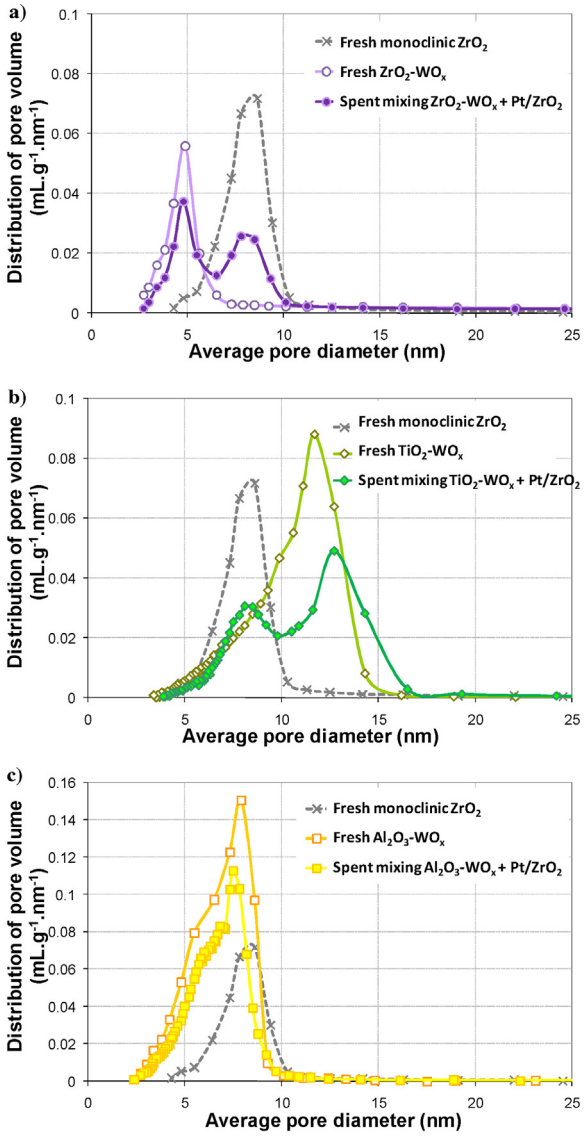

Fig. 6. Pore size distributions of (a) ZrO_2–WO_x, (b) TiO_2–WO_x, and (c) Al_2O_3–WO_x, for the fresh and spent catalysts (mixed with Pt/ZrO_2), in comparison with the oxide support ZrO_2 (monoclinic).

The elementary analysis of the spent mechanical mixings does not show any clear evidence of tungsten or platinum leaching. Moreover, the low carbon content (>0.3 wt.%) shows that nearly no coke is formed during the test, in accordance with previous results [19]. The textural modifications of the tungstated oxides (BET surface area, porous volume, and pore diameter) are limited, unlike what was previously observed on a Pt/SiO_2–Al_2O_3 catalyst [18]. In Fig. 6, the pore size distributions of the fresh monofunctional catalysts and of the spent mechanical mixtures are superposed. It is obvious that the porosity of the tungstated oxides is preserved during the test. The crystalline phases observed by XRD are also the same before and after test (Tables 1 and 2).The tungstated oxides thus seem to be stable in a hydrothermal reaction medium after 70 h on stream. It is important to note that some characterizations (NH_3-TPD and Raman) were not performed because of the presence of the metallic catalyst in the mechanical mixture. It is therefore impossible to determine the behavior of the tungsten species during the test, in particular regarding the dispersion, the oxidation state or the tungsten support interaction.

3.3. Sorbitol transformation

The tungstated oxides were tested using a mechanical mixing with the 2.2 wt.% Pt/ZrO_2 metallic catalyst. The absence of acid activity was verified using the cyclohexanol dehydration test described previously. As a consequence, the ZrO_2 support was not taken into account in the WHSV calculation. For example, the mechanical mixture Pt/ZrO_2 + SiO_2–Al_2O_3 (2 g + 4 g) are considered

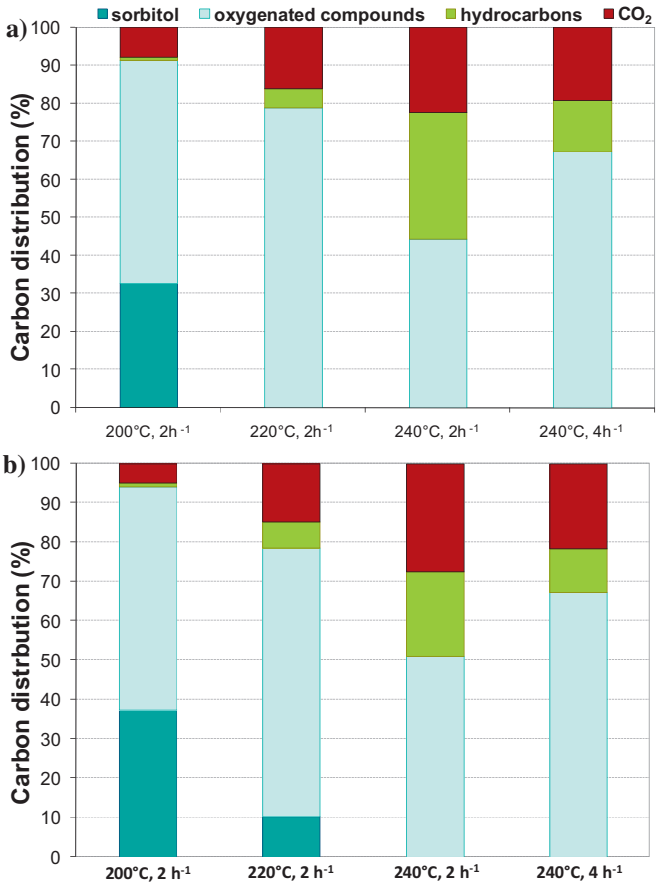

Fig. 7. Carbon distribution in the global effluent of sorbitol transformation over mechanical mixtures: (a) Pt/SiO_2–Al_2O_3 + SiO_2–Al_2O_3 and (b) Pt/ZrO_2 + SiO_2–Al_2O_3, at various operating conditions.

Table 2
Physical and chemical properties of the tungstated oxides and of the reference silica–alumina in mechanical mixing with 2.2 wt.% Pt/ZrO_2 after the sorbitol transformation test.

Mechanical mixing	$Pt/ZrO_2 + ZrO_2–WO_x$	$Pt/ZrO_2 + TiO_2–WO_x$	$Pt/ZrO_2 + Al_2O_3–WO_x$	$Pt/ZrO_2 + SiO_2–Al_2O_3$
Elementary analysis (wt.%)	0.76% Pt (0.73) 64% Zr (69) 7.6% W (5) 0.4% C	0.69% Pt (0.73) 23% Zr (25) 7.1% W (6) 35% Ti (35) <0.3% C	0.67% Pt (0.73) 24% Zr (25) 5% W (6) 35% Al (32) 0.4% C	0.57% Pt (0.73) 19% Zr (25) 27% Al (25) 14% Si (9) nd% C
Crystalline phase	ZrO_2 monoclinic + tetragonal	TiO_2 rutile + ZrO_2 monoclinic	γ-Al_2O_3 + ZrO_2 monoclinic	γ-Al_2O_3 + kaolinite + ZrO_2 monoclinic
BET surface area ($m^2\ g^{-1}$)	85 (75)	92 (96)	174 (183)	185 (238)
Pore volume ($mL\ g^{-1}$)	0.21	0.31	0.36	0.45

The values into brackets are the theoretical values of fresh mechanical mixings, calculated from the values obtained on monofunctional components of the mixing.

as 4.044 g in the WHSV calculation (0.044 g of platinum + 4 g of $SiO_2–Al_2O_3$).

The comparison of the acid catalysts was realized using the same mass of each acid catalyst and the same operating conditions. This gave us the possibility to study the influence of the specific surface area and the tungsten dispersion as determined by Raman analysis on reactivity. The absence of external diffusion limitations was verified with a $Pt/SiO_2–Al_2O_3$ catalyst; the other mesoporous catalysts are supposed to follow the same trend. The intra-granular diffusion limitations are supposed to be limited given the pore size. The mechanical mixture are noted Pt/ZrO_2 + AC (AC: "Acid phase" = $SiO_2–Al_2O_3$, $ZrO_2–WO_x$, $TiO_2–WO_x$, $Al_2O_3–WO_x$).

3.3.1. Validation of the mixing method

The mixing method was validated by comparing two catalytic systems, one with the platinum deposited on the acid phase (2.4 wt.%$Pt/SiO_2–Al_2O_3$ + $SiO_2–Al_2O_3$ (50:50) [19]) and one with the platinum deposited on the non active ZrO_2 (2.2 wt.%Pt/ZrO_2 + $SiO_2–Al_2O_3$). The overall platinum to $SiO_2–Al_2O_3$ mass ratio is the same on both catalysts (0.012).

Fig. 7 presents the global carbon distribution in the effluent for these two catalytic systems. The mechanical mixture (Fig. 7b) is slightly less active than $Pt/SiO_2–Al_2O_3$ + $SiO_2–Al_2O_3$ (Fig. 7a), but the products distributions are similar. At 240 °C, WHSV = 2 h^{-1}, the hydrocarbon part decreases to CO_2's advantage when the $Pt/SiO_2–Al_2O_3$ + $SiO_2–Al_2O_3$ system is replaced by Pt/ZrO_2 + $SiO_2–Al_2O_3$. One of the rate-limiting steps of sorbitol transformation is the dehydration–hydrogenation of remaining mono-alcohols into hydrocarbons. This reaction seems to be sensitive to the distance between acid and metallic sites. The primary alcohols undergo dehydrogenation–decarbonylation reactions faster than dehydration–hydrogenation when the distance between acid and metallic sites is important. Indeed, alcohols or hydrocarbons are formed by hydrogenation of unsaturated compounds on a metallic site; dehydration requires a long transfer to the acid sites whereas dehydrogenation–decarbonylation occurs on a metallic site too.

It is interesting to note that the same phenomenon occurs in the carbon distribution within hydrocarbons (Fig. S3): the distributions obtained for both catalytic systems are the same except at 240 °C, 2 h^{-1}, where the selectivity in C5-C6 hydrocarbons is lower for Pt/ZrO_2 + $SiO_2–Al_2O_3$.

In the carbon distribution within mono-alcohols and moreover in the carbon distribution in the overall aqueous phase, no difference is observed between both catalytic systems.

The comparison between $Pt/SiO_2–Al_2O_3$ + $SiO_2–Al_2O_3$ and Pt/ZrO_2 + $SiO_2–Al_2O_3$ shows that the mechanical mixing protocol is adapted to the sorbitol transformation reaction. However, when the reaction extent is maximal, i.e., at 240 °C, 2 h^{-1}, the competition between dehydration–hydrogenation (C—O cleavage) and dehydrogenation–decarbonylation (C—C cleavage) is modified by the long distance between metallic and acid sites: the C—C cleavage is favored in these conditions, leading to a slightly lower yield in C5-C6 hydrocarbons and a slightly higher CO_2 yield. Nevertheless,

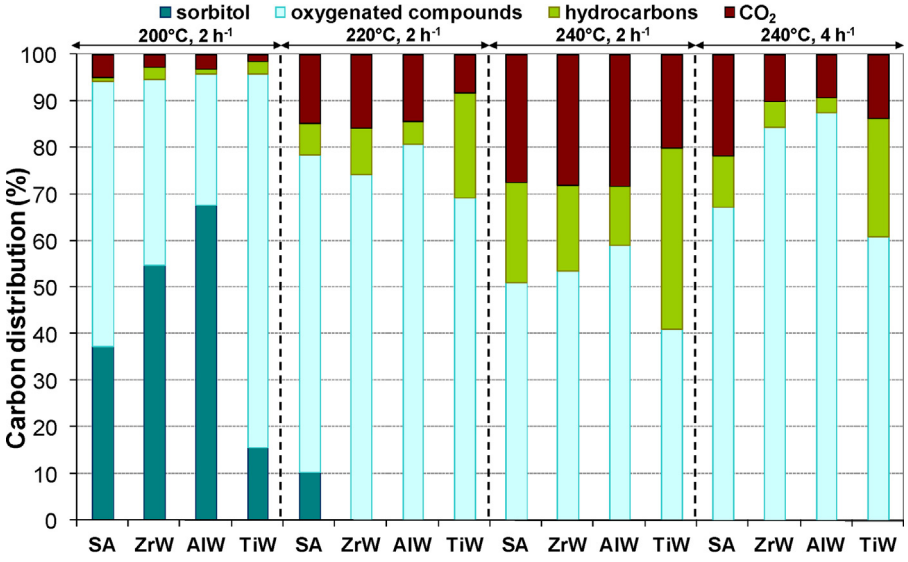

Fig. 8. Carbon distribution in the global effluent of sorbitol transformation over the mechanical mixtures: Pt/ZrO_2 + $SiO_2–Al_2O_3$ (SA), Pt/ZrO_2 + $ZrO_2–WO_x$ (ZrW), Pt/ZrO_2 + $Al_2O_3–WO_x$ (AlW), and Pt/ZrO_2 + $TiO_2–WO_x$ (TiW) at various operating conditions.

this phenomenon is not important enough to disturb the comparison of the acid solids in mechanical mixings.

3.3.2. Comparison of the tungstated oxides

Fig. 8 depicts the global carbon distributions obtained with four different mechanical mixings associating Pt/ZrO_2 with SiO_2–Al_2O_3, ZrO_2–WO_x, TiO_2–WO_x or Al_2O_3–WO_x. The first main difference concerns the sorbitol conversion at 200 °C. In the literature, the two first steps of sorbitol transformation are two cyclodehydration reactions, giving anhydrosorbitol, and then isosorbide [13]. Sorbitol conversion is thus correlated with the acid activity of the bifunctional catalytic systems, even if the further steps of the mechanism influence the conversion too. The solid acids' ranking by decreasing conversion at 200 °C is as follows:

$$TiO_2 - WO_x > SiO_2 - Al_2O_3 > ZrO_2 - WO_x > Al_2O_3 - WO_x.$$

This ranking is different from the one obtained during the model acidity test in water, which was:

$$ZrO_2 - WO_x \approx TiO_2 - WO_x > SiO_2 - Al_2O_3 > Al_2O_3 - WO_x.$$

Indeed, the ZrO_2–WO_x catalyst is not as active as expected. The major difference between these two catalytic tests is exposure time to hydrothermal conditions: the cyclohexanol dehydration test measures the activity during the first thirty minutes after water-catalyst contact whereas the results of the sorbitol transformation test are obtained after about twelve hours in hydrothermal conditions. A deactivation of the ZrO_2–WO_x catalyst is thus possible. An occupation or even a neutralization of acid sites by water is suspected, as described in literature for reactions in gas phase [34] or in liquid phase [35]. The presence of intermediates compounds with chelating properties and/or the acid reaction medium can also play a role in the observed differences.

In the case of tungstated alumina, a very low activity was observed during the cyclohexanol dehydration test. However, during the sorbitol transformation test, the conversion is important (32%) even if it is lower than for the other acid solids. This shows that the polyols are more easily dehydrated than the mono-alcohols, as reported in the literature [36].

Concerning selectivity, the fraction of oxygenated compounds follows the sorbitol conversion discussed earlier and the hydrocarbon yield is very low. Few gaseous products are formed. The CO_2 part is generally not much influenced by the nature of the solid acid phase, which confirms that CO_2 comes from decarbonylation/decarboxylation reactions catalyzed by platinum. However, in the case of TiO_2–WO_x, the CO_2 part is always lower than for the other acid solids and the hydrocarbon/CO_2 ratio is always higher whatever the operating conditions, evidencing a positive effect of tungstated oxide on the C—C/C—O cleavage competition.

The temperature increases until 240 °C (WHSV 2 h^{-1}) that leads to an increase of CO_2 and hydrocarbons parts at the expense of the oxygenated compounds, in all cases. The hydrocarbon part is different from one acid solid to another and the ranking by decreasing hydrocarbon yield is the following:

$$TiO_2 - WO_x > ZrO_2 - WO_x \approx SiO_2 - Al_2O_3 > Al_2O_3 - WO_x.$$

The effect of space velocity depends on the acid solid present in the mechanical mixing. The space velocity increase from 2 to 4 h^{-1} leads to a decrease of the hydrocarbon part in favor of the oxygenated compounds in all cases, without noticeable effect on CO_2 in the case of silica–alumina and with a decrease of the CO_2 part for the tungstated oxides.

The comparison of the global carbon distribution at several operating conditions evidences the specific behavior of TiO_2–WO_x, which leads to the highest reaction advancement degree, with a positive influence on the C—O/C—C cleavage competition.

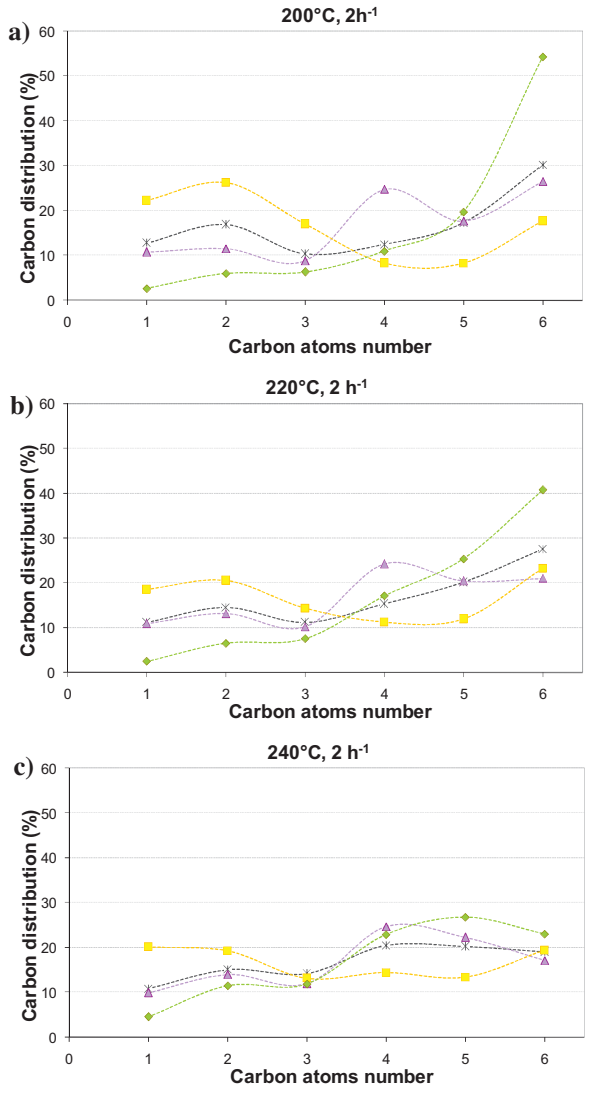

Fig. 9. Carbon distribution in the hydrocarbons during sorbitol transformation over mechanical mixtures $Pt/ZrO_2 + SiO_2$–Al_2O_3 (✱) $Pt/ZrO_2 + ZrO_2$–WO_x (▲), $Pt/ZrO_2 + Al_2O_3$–WO_x (■), and $Pt/ZrO_2 + TiO_2$–WO_x (♦) at various operating conditions: (a) 200 °C, 2 h^{-1}; (b) 220 °C, 2 h^{-1}; (c) 240 °C, 2 h^{-1}. The lines between the points are drawn to help the reader.

Fig. 9 depicts the carbon distribution within hydrocarbons according to their chain length at various operating conditions. ZrO_2–WO_x favors the formation of C4–C6 compounds; particularly C4 at 240 °C. Al_2O_3–WO_x seems to favor C1-C2 hydrocarbons. TiO_2–WO_x leads to a high selectivity in C6 hydrocarbons. This selectivity decreases slightly when the temperature increases. This confirms the importance of the competition between the exothermic C—O cleavage reactions and the endothermic C—C cleavage reactions. The temperature thus tends to favor the C—C cleavages.

Fig. 10 presents the carbon distribution within alcohols according to their chain length. The C2-C3 and C5-C6 compounds are the most represented. TiO_2–WO_x is the most selective in the long chain alcohols (C5-C6), even if this selectivity decreases when the temperature increases, whereas Al_2O_3–WO_x is the most selective in C2-C3 alcohols.

The detailed composition of the oxygenated compounds present in the aqueous phase (Table S4) is also dependent on the acid solid. Tungstated alumina leads to the highest alcohols part, particularly ethanol and 1-propanol. Tungstated titania and zirconia give fewer alcohols, but more long chain ketones and heterocycles,

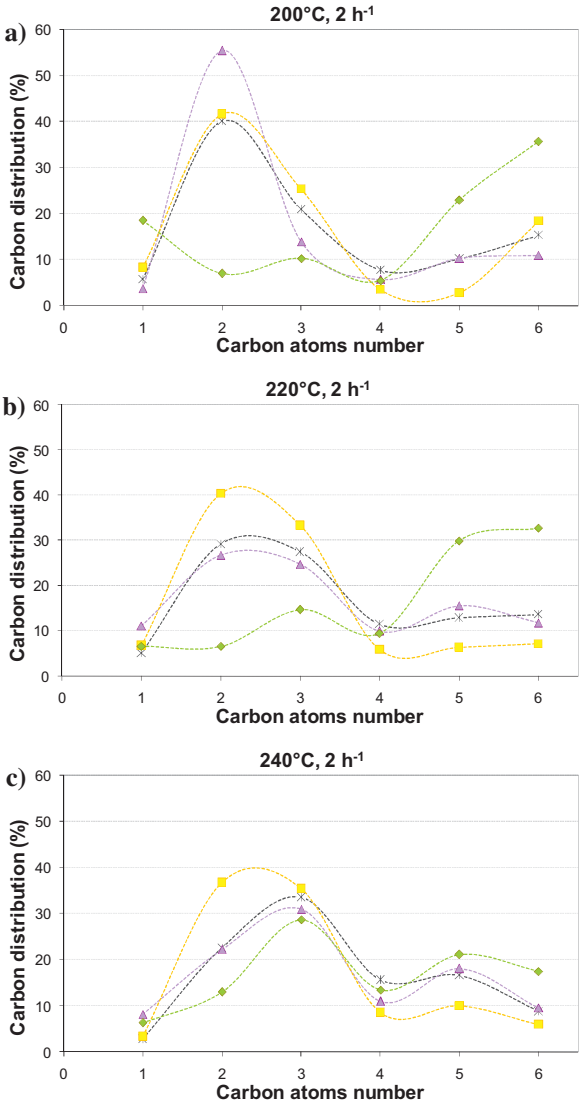

Fig. 10. Carbon distribution in the alcohols during sorbitol transformation over mechanical mixtures $Pt/ZrO_2 + SiO_2–Al_2O_3$ (✕), $Pt/ZrO_2 + ZrO_2–WO_x$ (▲), $Pt/ZrO_2 + Al_2O_3–WO_x$ (■), and $Pt/ZrO_2 + TiO_2–WO_x$ (♦) at various operating conditions: (a) 200 °C, 2 h^{-1}; (b) 220 °C, 2 h^{-1}; (c) 240 °C, 2 h^{-1}. The lines between the points are drawn to help the reader.

evidencing a lack of hydrogenation sites. These compounds represent a stock of potential long chain hydrocarbons: if the hydrogenation reaction advancement was higher, they would be hydrogenated in secondary alcohols and then dehydrated–hydrogenated into alkanes. No decarbonylation could occur since there is no terminal alcohol.

Finally, each tungstated oxide in mechanical mixing with Pt/ZrO_2 leads to a specific selectivity. Tungstated zirconia does not increase the activity of the bifunctional catalytic system during sorbitol transformation, whereas its activity for monoalcohol dehydration in liquid water is high. An acid sites deactivation is possible; particularly a sintering of the polytungstate dispersed species would not be surprising in the aqueous reaction medium. The performances of $ZrO_2–WO_x$ are close to $SiO_2–Al_2O_3$ reference acid catalyst. Tungstated titania leads to an increased hydrocarbon yield, particularly with long chain, and to a decreased CO_2 yield, showing that the C—C/C—O cleavage competition is modified by the acid activity. The presence of strong acid sites, active in water, is responsible for this improvement. The detailed analysis of the oxygenated compounds evidences a lack of hydrogenation sites. The activity of the overall bifunctional catalytic system could be improved by using a hydrogenating metallic phase more active than Pt/ZrO_2. Tungstated alumina is mildly active during sorbitol transformation; a significant part of this activity could be attributed to C—C cleavage reaction such as retro-aldol reaction, leading to a high selectivity in C2-C3 compounds. This kind of reaction could be catalyzed by basic sites present at the alumina surface. Lewis acid sites can also form L-OH- Brønsted basic sites in association with water, as previously suggested [37]. Unless this selectivity was not expected here, the production of short alcohols (ethanol and propanols) is interesting in a biorefinery context.

4. Conclusion

The objective of the present study was to transform selectively sorbitol into gasoline-like hydrocarbons (C5-C6 alkanes) which represents a promising opportunity for the future energy supply. Three tungsten-based catalysts have been prepared for sorbitol transformation in aqueous phase. Their comparison when tested in mechanical mixing with Pt/ZrO_2 shows that products yields are dependent on the nature of the acid solid: the tungstated alumina leads to high yields in short alcohols whereas the tungstated titania gives high yields in long chain hydrocarbons. The correlations between tungsten species, acidity in gas phase and acidity in aqueous phase are complex. The strong tungsten-support interactions observed on $ZrO_2–WO_x$ does not seem to favor the formation of strong acid sites. However, $TiO_2–WO_x$ contains less condensed tungsten species and an important amount of strong acid sites. This allows us to propose that the strong acid sites are due to highly dispersed tungsten species with medium to weak tungsten-support interactions. The acid activity in water seems to be correlated with the presence of strong acid sites. Weak acid sites, even when they are numerous, are not active in water. This can be due to an adsorption of water molecules on the weak acid sites.

$TiO_2–WO_x$ is thus the optimal acid phase for the conversion of sorbitol into valuable hydrocarbons. Furthermore, the bifunctional $Pt/ZrO_2–TiO_2–WO_x$ catalytic system is stable in hydrothermal conditions. This catalytic system represents a promising tool to produce fuels from sugars in a biorefinery context. Some mechanistic considerations are still on interest about these promising systems.

Acknowledgments

The authors gratefully thank Nadège Charon for her help in the development of products analysis methods, Olivier Delpoux for his help in Raman spectroscopy, Agnès Le Masle and the HPLC laboratory for the HPLC analyses and the Solids Characterizations department for the solid analyses. This work was supported by IFPEN.

Appendix A. Supplementary data

Supplementary material related to this article can be found, in the online version, at http://dx.doi.org/10.1016/j.apcatb.2013.11.016.

References

[1] E. Thomas, Science 285 (1999) 1209.
[2] G.W. Huber, J.N. Chheda, C.J. Barrett, J.A. Dumesic, Science 308 (2005) 1446–1450.
[3] G.W. Huber, R.D. Cortright, J.A. Dumesic, Angew. Chem. Int. Ed. 43 (2004) 1549–1551.
[4] G.W. Huber, J.A. Dumesic, Catal. Today 111 (2006) 119–132.
[5] T. Werpy, G.R. Petersen, in: DOE (Ed.), Topvalue Added Chemicals from Biomass, U.S. Department of Energy, Washington, DC, 2004 (top 12).
[6] J.J. Bozell, G.R. Petersen, Green Chem. 12 (2010) 539–554.
[7] B. Kusserow, S. Schimpf, P. Claus, Adv. Synth. Catal. 345 (2003) 289–299.

[8] P. Gallezot, N. Nicolaus, G. Flèche, P. Fuertes, A. Perrard, J. Catal. 180 (1998) 51–55.
[9] A. Shrotri, A. Tanksale, J.N. Beltramini, H. Gurav, S.V. Chilukuri, Catal. Sci. Technol. 2 (2012) 1852–1858.
[10] D. Weiping, T. Xuesong, F. Wenhao, Z. Qinghong, W. Ye, Catal. Lett. 133 (2009) 167–174.
[11] L.-N. Ding, A.-Q. Wang, M.-Y. Zheng, T. Zhang, ChemSusChem 3 (2010) 818–821.
[12] L. Vilcocq, A. Cabiac, C. Especel, E. Guillon, D. Duprez, Oil Gas Sci. Technol. e-publication (2013), http://dx.doi.org/10.2516/ogst/2012073.
[13] N. Li, G.W. Huber, J. Catal. 207 (2010) 48–59.
[14] T.P. Vispute, G.W. Huber, Green Chem. 11 (2009) 1433–1445.
[15] R.M. West, M.H. Tucker, D.J. Braden, J.A. Dumesic, Catal. Commun. 10 (2009) 1743–1746.
[16] N. Li, G.A. Tompsett, G.W. Huber, ChemSusChem 3 (2010) 1154–1157.
[17] Q. Zhang, K. Qiu, B. Li, T. Jiang, X. Zhang, L. Ma, T. Wang, Fuel 90 (2011) 3468–3472.
[18] L. Vilcocq, A. Cabiac, C. Especel, S. Lacombe, D. Duprez, Catal. Commun. 15 (2011) 18–22.
[19] L. Vilcocq, A. Cabiac, C. Especel, S. Lacombe, D. Duprez, Catal. Today 189 (2012) 117–122.
[20] R.M. Ravenelle, F. Schuber, A. D'Amico, N. Danilina, J.A. van Bokhoven, J.A. Lercher, C.W. Jones, C. Sievers, J. Phys. Chem. C 114 (2010) 19582–19595.
[21] R. Dimitrijevic, W. Lutz, A. Ritzmann, J. Phys. Chem. Solids 67 (2006) 1741–1748.
[22] R.M. West, D.J. Braden, J.A. Dumesic, J. Catal. 262 (2009) 134–143.
[23] R. Weingarten, G.A. Tompsett, J. Conner, G.W. Huber, J. Catal. 279 (2011) 174–182.
[24] F. Chambon, F. Rataboul, C. Pinel, A. Cabiac, E. Guillon, N. Essayem, Appl. Catal. B 105 (2011) 171–181.
[25] A. Pottier, C. Chaneac, E. Tronc, L. Mazerolles, J.-P. Jolivet, J. Mater. Chem. 11 (2001) 1116–1121.
[26] S. Loridant, C. Feche, N. Essayem, F. Figueras, J. Phys. Chem. B 109 (2005) 5631–5637.
[27] D. Barton, S. Soled, E. Iglesia, Top. Catal. 6 (1998) 87–99.
[28] I.E. Wachs, C.A. Roberts, Chem. Soc. Rev. 39 (2010) 5002–5017.
[29] M.E. Manriquez, T. Lopez, R. Gomez, J. Navarrete, J. Mol. Catal. A: Chem. 220 (2004) 229–237.
[30] B.M. Reddy, P.M. Sreekanth, V.R. Reddy, J. Mol. Catal. A: Chem. 225 (2005) 71–78.
[31] M. Watanabe, Y. Aizawa, T. Iida, R. Nishimura, H. Inomata, Appl. Catal. A 295 (2005) 150–156.
[32] P. Carniti, A. Gervasini, M. Marzo, Catal. Today 152 (2010) 42–47.
[33] H. Wang, Y. Wu, L. He, Z. Liu, Energy Fuels 26 (2012) 6518–6527.
[34] A. Corma, O. Marie, F.J. Ortega, J. Catal. 222 (2004) 338–347.
[35] J.M. Heras, L. Viscido, Catal. Rev. 30 (1988) 281–338.
[36] B. Peng, C. Zhao, I. Mejia-Centeno, G.A. Fuentes, A. Jentys, J.A. Lercher, Catal. Today 183 (2012) 3–9.
[37] F. Chambon, F. Rataboul, C. Pinel, A. Cabiac, E. Guillon, N. Essayem, ChemSusChem 6 (2013) 500–507.